Laser Investigations with Zemax OpticStudio

ISAAC WOODARD[1]

[1] *Knight Campus Graduate Internship Program, University of Oregon, 1252 University of Oregon, Eugene OR 97403*
[*] *isaac.j.woodard@gmail.com*

Abstract: Three systems using a HeNe laser input were analyzed to explore some of the features of Zemax OpticStudio. The first system was a laser polygon scanner designed to scan a 5 mm diameter beam through 10°. Loss of spot shape was minimal for ±2.5° scan angles but significant for ±4.4°. The second system compared the single-mode fiber coupling efficiencies of two Thorlabs lenses for a 3 mm beam. Coupling was higher for the more powerful lens but both lenses had spot sizes much greater than the fiber core. The third system used a Mach-Zehnder interferometer to compare measurements of index of refraction change for a temperature modulated silica sample with and without thermal expansion considered. Addition of thermal expansion effects gave a change of less than 10% in the measurements.

1. Introduction

1.1. Polygon Scanner

Scanning laser systems see a wide range of uses, such as laser printing, drilling and scanning microscopy [1, 2]. These systems come in three general types: objective, post-objective, and pre-objective [1]. Objective scanning can be accomplished simply by moving a focusing lens to deflect the beam. The other two types of scanning use a mirror to deflect the beam either after being focused (post-objective) or before being focused (pre-objective).

An example of a pre-objective laser scanning system is a polygon scanner. A polygon scanner is a mirror with at least three reflective surfaces which can be used to deflect a laser beam by rotating the polygon scanner about its center [1]. Shown in Fig. 1 is a polygon scanner in the shape of a regular octagon. Polygon scanners are most seen in applications requiring high scan rates or large scan angles [1].

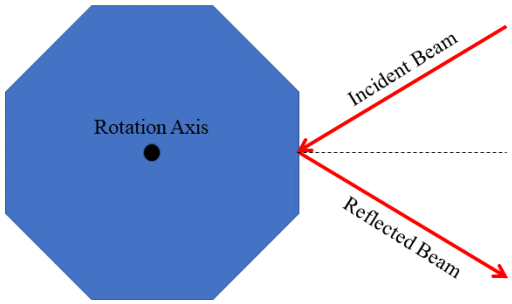

Fig. 1. Concept diagram for a regular octagonal polygon scanner.

For the first investigation, a polygon scanner system was designed to scan through an angle of 10° for a 5 mm HeNe input. The focusing lens was set to an F number of 3 and was optimized to minimize RMS spot size.

An important property of scanning systems is to avoid changes in spot size at different scan angles. Because a spherical lens was used to focus the beam, aberrations in the beam can be expected to increase with the scan angle. These aberrations will lead to the spot becoming elliptical in shape [2].

1.2. Single-Mode Fiber Coupling

Single-mode fibers are designed to transmit a single mode of light for a certain range of wavelengths. The advantages of single-mode fiber coupling over multi-mode include no modal dispersion, reduction in modal noise, and lower power attenuation [3]. This makes single-mode fibers ideal for applications requiring transmission of high data rates over large distances.

Fiber coupling is often performed with a laser source. A laser beam can be modeled with a Gaussian irradiance profile which expands hyperbolically as it propagates through space. Width of the beam is often defined at the point in the profile where the intensity drops off by a factor of $1/e^2$ [4]. The minimum width of the profile is known as the waist and occurs somewhere within the laser body.

To couple a beam into a fiber it must be focused so that a new waist is created at the opening to the fiber as shown in Fig. 2. For a single-mode fiber the core is small enough to allow only one mode to enter the fiber. The physical extent of the core diameter is generally different from the mode field diameter which specifies the size of the beam profile which can "fit" in the fiber [4].

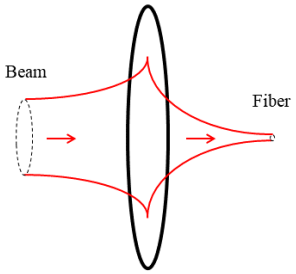

Fig. 2. A beam from a laser diverges before being focused to a smaller waist size by a lens. The focused waist size is ideally equal to the mode field diameter of the fiber.

Coupling effiency is the portion of the energy from the beam which enters the fiber,

$$\text{Coupling Efficiency} = \frac{\text{Fiber Energy}}{\text{Beam Energy}}. \tag{1}$$

Losses due to absorption and reflection weren't considered in the model so the beam energy is unchanged after being focused by the lens.

An LA1251 and LA1252 lens from the Thorlabs catalogue were used to couple into a Thorlabs 630HP single-mode fiber. The goal was to maximize coupling efficiency while minimizing cost.

1.3. Mach-Zehnder Interferometer

A Mach-Zehnder interferometer splits light down two independent optical paths before re-combining them to create an interference pattern. The independence of the two paths allows measurements to be made on the thickness or index of refraction of a sample placed in one of the paths. For path length differences equal to an integer multiple of the source wavelength, constructive interference will be observed. Otherwise some amount of destructive interference will be observed.

The phase shift for a certain optical path length difference and wavelength is given by [5],

$$\delta = 2\pi \frac{l_1 - l_2}{\lambda}. \tag{2}$$

In the case of a sample with uniform thickness and index of refraction n, the interference pattern will be a spot. A bright spot indicates constructive interference and a dark spot indicates

destructive interference. A shift from a bright to a dark spot corresponds to a phase shift of π. Defining l_2 as $l_1 + nd$ and considering the case of a π phase shift gives,

$$nd = \frac{\lambda}{2}, \tag{3}$$

where d is the change in thickness of the sample. By finding the change in thickness required to shift the output from a bright to a dark spot, the sample index of refraction can be calculated.

Thermal changes in a sample generally lead to two sources of variation in the optical path length: index of refraction and expansion. Thermal variations in index of refraction can be modeled in OpticStudio by activating them in the Environment menu. This also allows thermal expansion to be modeled based on the thermal coefficient of expansion (TCE) for a material by adding a thermal pickup solve in the multi-configuration editor [6].

The goal of this investigation is to determine how much error can be expected in measuring the change in index of refraction of a silica sample if thermal expansion effects are ignored. Expansion effects can be separated into the individual effect of the expansion and the cross effect between the expansion and index of refraction change.

2. Experiment

2.1. Polygon Scanner

The process for designing a polygon scanner system is outlined in the Zemax knowledgebase article "How to model a scanning mirror" [7]. The article along with its "Starting Point" file were used to design a polygon scanner with the specifications outlined in the Introduction.

The first step was to add a tiltable mirror to the system. This required adding coordinate breaks to the system to modify the coordinate system for the mirror and the reflected rays. Conveniently, OpticStudio has tools for adding mirrors and tilting elements. The "Add Fold Mirror" tool and "Tilt/Decenter Elements" tools in the lens data editor were used to reflect the rays 90° and tilt the mirror ±5° through the YZ plane.

The second step was to convert the mirror to a polygon mirror. This was done by modifying the thicknesses of the first three coordinate breaks and the mirror surface to move the rotation axis 20 mm behind the mirror while keeping the mirror at the same starting position. Multiple configurations were defined to show the neutral and extreme scan angles as seen in Fig. 3.

The main modifications from the example outlined in the article were a reduction in the entrance pupil diameter (EPD) to model the laser diameter, a change in the F number, and a reduction in the mirror-to-lens distance. The reduction in distance was necessary to keep the geometry of the lens physical after changing the EPD and F number.

To optimize the system for RMS spot size, the front radius, front thickness, and back thickness of the lens were set to variable. A minimum glass boundary of 2.0 mm, maximum of 30.0 mm, and minimum edge thickness of 2.0 mm were set to keep the lens design manufacturable. The sample file came preset with an aperture margin of 2.0 mm to allow for mounting the lens.

2.2. Single-Mode Fiber Coupling

Three different tools were identified for analyzing coupling efficiency: Paraxial Gaussian Beam, Single Mode Coupling, and Physical Optics Propagation (POP). After testing each tool, POP was selected as the method of choice. Using Physical Optics Propagation provides the most robust analysis and allows both optimization and coupling efficiency measurements to be made with the POPD operand [8].

To set up the system for coupling, the entrance pupil diameter was set to 3.0 mm and the wavelength was set to 632.8 nm to represent the HeNe beam. Apodization of the beam was set to Gaussian with a scale factor of 1.0 to better model a real HeNe beam. This had the effect of modifying the entrance aperture to shift the beam's energy towards the center of the beam [9].

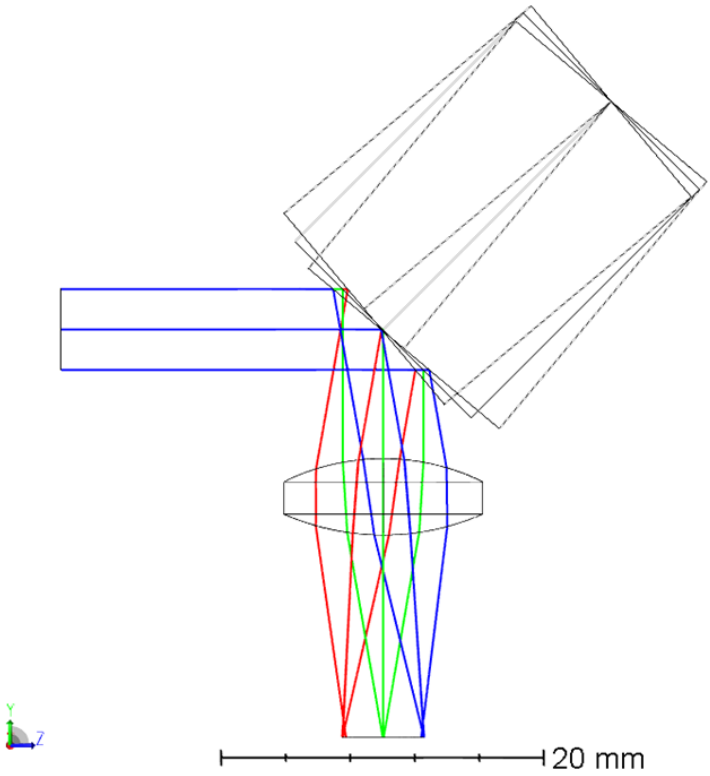

Fig. 3. Top-down view of the polygon scanner system with three scan angle configurations shown: -5° (blue), 0° (green), 5° (red).

The opening to the fiber was represented with a planar surface in the image plane with a diameter equal to the core diameter of the fiber.

The single-mode fiber chosen for coupling was Thorlabs' 630HP fiber. This fiber has a core diameter of 3.5 µm, a mode field diameter of 4.0 ± 0.5 µm for a 630 nm beam, and a numerical aperture of 0.13 [10]. Coupling was first attempted with a Thorlabs LA1251 lens having an effective focal length (EFL) of 99.98 mm. The lens was inserted using the OpticStudio lens catalogue 5.0 mm from the beam source.

At this point the system was prepared for optimization. In the POP settings the beam was defined with a waist radius of 1.5 mm and the fiber was defined with a waist radius of 2.0 µm based on the mode field diameter for the 630HP fiber. Saving these settings allowed a POPD operand to be used to optimize the system for coupling efficiency and report the value achieved. The variable to be optimized was the distance from the lens to the fiber. It was found that a Quickfocus optimization was necessary before running the merit function to get the system close to the ideal distance.

The LA1251 lens showed poor coupling efficiency after optimization, so the system was also tested with an LA1252 lens having an EFL of 25.43 mm. A FICL operand was added to compare the coupling efficiency reported by the POP analysis to the value reported by the Single Mode Coupling tool.

2.3. *Mach-Zehnder Interferometer*

A sequential sample file packaged with OpticStudio was used for the initial design of the Mach-Zehnder interferometer. A topdown view of the design with some modifications can be seen in Fig. 4. The position of the output lens for the bottom arm was adjusted to center on the beam and the thickness of the second beam splitter was changed to more closely match the thickness of the first beam splitter. The wavelength of the input was changed to the 632.8 nm HeNe preset.

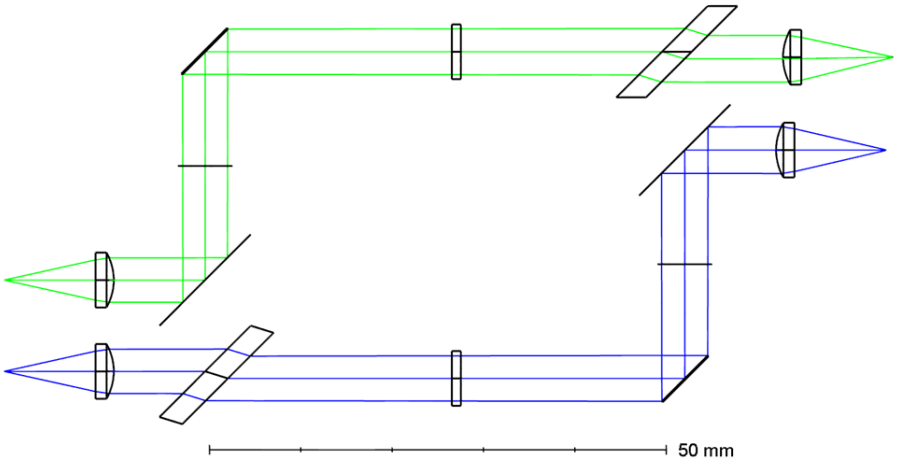

Fig. 4. Topdown view of the layout for a Mach-Zehnder interferometer designed in OpticStudio. In this design the two arms are defined in separate configurations indicated by the ray color. Interference effects are modeled by combining the outputs from each configuration.

The sample was modeled as a standard surface just before the combining beamsplitter in the upper arm. Changing the material to silica required first loading in the MISC materials catalogue. A TEMP operand was added to the multi-configuration editor to allow the temperture of the sample to be adjusted independently.

Phase shifts were determined by inspecting the display of the interferogram tool. By checking the box for "consider path length difference" and selecting the image planes for both arms of the interferometer, the interferogram displayed the interference between the two paths. Example interferograms for constructive and destructive interference are shown in Fig. 5. In addition to the graphical display, text values of the intensity were used for fine-tuning.

The interferogram display was used to find changes in thickness and temperature which caused a phase shift of π. Thickness was first adjusted at constant temperature. Temperature was then adjusted for sample thicknesses of 1 mm and 2 mm with only changes in index of refraction modeled. The temperature measurement were then repeated with thermal expansion effects added. Care was taken to ensure measurements were made within a single cycle.

3. Results & Analysis

3.1. *Polygon Scanner*

The range of the scanning system in the image plane was slightly more than the desired ±5° due to additional deflection by the focusing lens. For scanner deflection angles of ±5° the shift in the beam position in the image plane was roughly ±2.5 mm. With a mirror-to-image distance of 25 mm, the total deflection angle was ±5.7°.

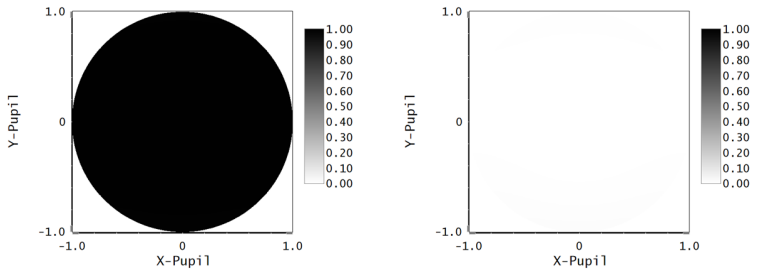

Fig. 5. Example interferograms from OpticStudio showing constructive interference (left) and destructive interference (right). Taken using 1024x1024 sampling and the silica thicknesses from column 2 of Table 2.

It was found that a scan angle of ±4.4° gave a total deflection angle of ±5.0°. Significant aberrations were found at the extreme scanning angles, so analysis was restricted to total deflection angles of ±5.0°. The spot diagrams for five different scan angles in this range are shown in Fig. 6.

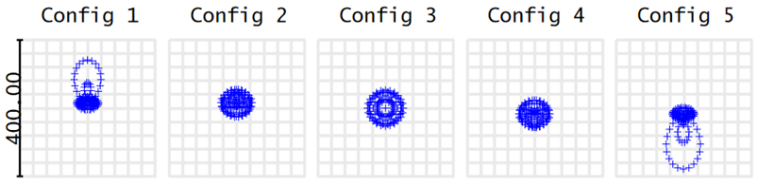

Fig. 6. Spot diagram for scan angles of (left to right) -4.4°, -2.5°, 0°, 2.5°, and 4.4°. Units are μm.

For a scan angle of 0° the aberrations are symmetric about both the X and Y axis. As the scan angle increases the spot elongates along the X axis and is no longer symmetric about the Y axis. At the edge of the scan range the focus quality deteriorates significantly and the spot grows a comet-like tail.

We can examine the aberrations for the extreme scan angles more closely by inspecting their ray fan diagrams. For spherical aberrations the ray fan should have a cubic shape, for comatic aberrations a parabolic shape, and for astigmatic abberations a tilt corresponding to a separation in focus of the tangential and sagittal rays [11]. The ray fans for the extreme scan angles shown in Fig. 7 appear to be a sum of these three aberrations. In addition, we can see the ray fans are not quite symmetrical about the horizontal axis.

3.2. Single-Mode Fiber Coupling

The coupling efficiencies and costs of each system are reported in Table 1. The LA1252 lens showed roughly an eight-fold increase in efficiency with a difference of only $3.57 in cost and a smaller spacing between the lens and fiber.

This increase in coupling efficiency can be understood by looking at the diffraction point-spread function diagrams in Fig. 8. The diffraction intensity at the surface of the fiber has a similar pattern for both lenses, but the scale is about four times smaller for the LA1252 lens. An increase in efficiency of more than four times is likely due to the Gaussian profile of the beam concentrating more energy towards the center. Both lenses, however, appear to have insufficient power to focus the beam to a spot size comparable to the 3.5μm core diameter of the fiber.

There is a large difference between the coupling efficiencies of the POPD and FICL operands. While this raises doubt on quantitative accuracy, qualitative comparisons appear unaffected.

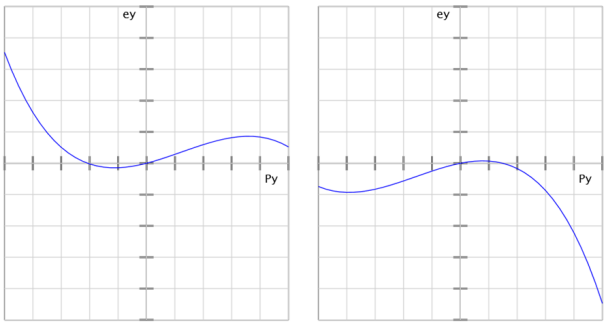

Fig. 7. Ray fans for scan angles of -4.4° (left) and 4.4° (right). Max scale is ±200 µm for both.

Table 1. Summary of coupling efficiencies for both lenses using the POPD and FICL operands. Distance is the optimized lens-to-fiber spacing. Cost is the price of the lens plus the base price of the fiber per meter.

Lens	EFL (mm)	Distance (mm)	POPD Eff.	FICL Eff.	Cost
LA1251	99.98	97.65	0.085	0.026	$23.27 + $6.00/m
LA1252	25.43	18.26	0.627	0.288	$26.84 + $6.00/m

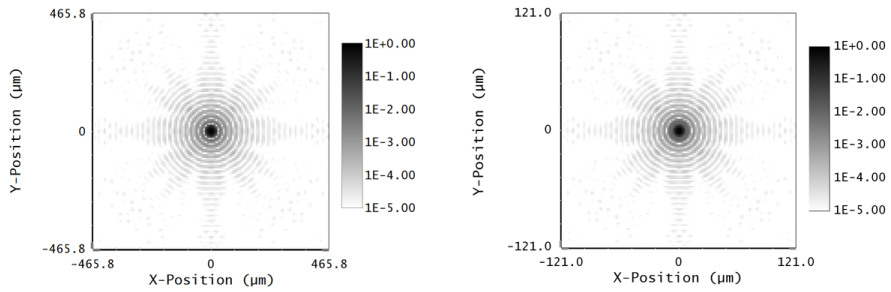

Fig. 8. Diffraction point-spread functions in the plane of the fiber using the LA1251 lens (left) and the LA1252 lens (right).

3.3. Mach-Zehnder Interferometer

The measurements of thickness and temperature corresponding to a phase shift of π are given in Table 2. Included are temperature differences for just the index of refraction model and the index of refraction with thermal expansion model.

Using the change in thickness and Eq. 3 gives an index of refraction of 1.44 at 20° (the software default). OpticStudio used a value of 1.4585 at 20 °C for the silica material. The measurement procedure accurately determined the correct index value to all but the last decimal place.

Adding thermal expansion to the model gives a change in temperature difference for a 1 mm sample of 8.45%. For the 2 mm sample the change is 8.28%. These percentages show thermal expansion has a much smaller effect on the optical path length than changes in index of refraction.

Careful inspection of the white interferogram in Fig. 5 shows the optical path length differnce isn't uniform in the XY plane. Pixels at the top and bottom of the display show less destructive interference. This indicates an asymmetry in the system about the X axis.

Table 2. Summary of thickness and temperature measurements of a silica sample for a change of one half-cycle in optical path length between the two arms of the interferometer. Temperature was adjusted for a 1 mm and 2 mm thick sample. The third and fifth columns were gathered without modeling thermal expansion. The fourth and sixth columns were gathered with thermal expansion effects included.

Interferogram	**Thickness (um)**	**T for 1 mm (°C)**		**T for 2 mm (°C)**	
Black	0.981	2.69	4.05	29.9	29.1
White	1.20	39.4	37.9	11.6	12.2
Difference	0.219	36.7	33.9	18.3	16.9

4. Conclusion

4.1. Polygon Scanner

The polygon scanning system was optmized over a range slightly more than the desired ±5°. However, significant changes to the spot shape at extreme scan angles indicate the useful range of the scanner may be smaller than ±5°.

Further investigations might be conducted to address this issue. Different glass choices could be explored to reduce aberrations from the focusing lens. This would likely involve designing a more complicated multi-lens system to reduce the net effect on the spot shape. It also could be worth exploring the mirror-to-lens distance and its effect on aberrations. While exploring the initial design, smaller distances seemed to lead to less aberrations.

4.2. Single-Mode Fiber Coupling

The higher power LA1252 lens showed much greater coupling efficiency for nearly the same cost as the LA1251 lens. However, both lenses showed spot sizes much larger than the core diameter of the fiber. A lens or multi-lens system with greater power should be tested.

There are improvements which could be made to the accuracy of the model. First, the cause of the difference between the coupling efficiencies measured by the POPD and FICL operands should be investigated. Second, the model could be modified to consider lens reflectivity and absorption. This would allow the effects of lens coatings to be explored and would be particularly important if a multi-lens focusing system was adopted.

4.3. Mach-Zehnder Interferometer

Measurement of the index of refraction for the silica indicates the interferometer design is working as expected. A change of less than 10% was found in temperature difference measurements made with and without thermal expansion effects. This suggests it is safe to ignore cross effects between the change in index of refraction and thermal expansion, and may validate ignoring thermal expansion effects entirely.

The results of this investigation could be extended to modeling a real experiment to measure index of refraction changes and thermal expansion of solid materials. Some additional complications would need to be considered. First, arbitrally changing the thickness of a sample might not be possible. Second, it could be difficult to isolate the temperature of the sample from the environment. Third, it would be necessary to decouple the index of refraction change and thermal expansion effects for precise measurements to be made.

References

1. G. E. S. Gerald F. Marshall, ed., *Handbook of Optical and Laser Scanning 2nd edition* (CRC Press, 2012).
2. R. Paschotta, "Scanning lenses," RP Photonics Encyclopedia, accessed on November 22, 2021.
3. B. E. A. Saleh and M. C. Teich, *Fundamentals of Photonics 2nd Edition* (John Wiley & Sons, 2007).
4. R. Paschotta, "Mode radius," RP Photonics Encyclopedia, accessed on November 26, 2021.
5. K. P. Zetie, S. F. Adams, and R. M. Tocknell, "How does a mach-zehnder interferometer work?" Phys. Educ. **35**, 46–48 (2000).
6. N.-H. Kim, "How to model thermal effects using opticstudio," (March 30, 2021). Retrieved from https://support.zemax.com/hc/en-us/articles/1500005576962-How-to-model-thermal-effects-using-OpticStudio.
7. M. Nicholson, "How to model a scanning mirror," (March 30, 2021). Retrieved from https://support.zemax.com/hc/en-us/articles/1500005576502-How-to-model-a-scanning-mirror.
8. M. Nicholson and K. Norton, "Single-mode fiber coupling in opticstudio," (March 30, 2021). Retrieved from https://support.zemax.com/hc/en-us/articles/1500005576542-Single-mode-fiber-coupling-in-OpticStudio.
9. M. Nicholson, "What does the term apodization mean?" (March 30, 2021). Retrieved from https://support.zemax.com/hc/en-us/articles/1500005486901-What-does-the-term-apodization-mean-.
10. Thorlabs, "Single mode fiber 630hp spec sheet," (November 29, 2017). Retrieved from https://www.thorlabs.com/thorproduct.cfm?partnumber=630HP.
11. H. Gross, ed., *Handbook of Optical Systems, Volume 1: Fundamentals of Technical Optics* (Wiley, 2005).